CHEMISTRY
A EUROPEAN JOURNAL

DOI: 10.1002/chem.200701514

Probing Defect Sites on TiO_2 with $[Re_3(CO)_{12}H_3]$: Spectroscopic Characterization of the Surface Species

Kongkiat Suriye,[a, b] Rodrigo J. Lobo-Lapidus,[a] Gregory J. Yeagle,[c] Piyasan Praserthdam,[b] R. David Britt,[c] and Bruce C. Gates*[a]

Abstract: Samples of the anatase phase of titania were treated under vacuum to create Ti^{3+} surface-defect sites and surface O^- and O_2^- species (indicated by electron paramagnetic resonance (EPR) spectra), accompanied by the disappearance of bridging surface OH groups and the formation of terminal Ti^{3+}–OH groups (indicated by IR spectra). EPR spectra showed that the probe molecule $[Re_3(CO)_{12}H_3]$ reacted preferentially with the Ti^{3+} sites, forming Ti^{4+} sites with OH groups as the $[Re_3(CO)_{12}H_3]$ was adsorbed. Extended X-ray absorption fine structure (EXAFS) spectra showed that these clusters were deprotonated upon adsorption, with the triangular metal frame remaining intact; EPR spectra demonstrated the simultaneous removal of surface O^- and O_2^- species. The data determined by the three complementary techniques form the basis of a schematic representation of the surface chemistry. According to this picture, during evacuation at 773 K, defect sites are formed on hydroxylated titania as a bridging OH group is removed, forming two neighboring Ti^{3+} sites, or, when a Ti^{4+}–O bond is cleaved, forming a Ti^{3+} site and an O^- species, with the Ti^{4+}–OH group being converted into a Ti^{3+}–OH group. When the probe molecule $[Re_3(CO)_{12}H_3]$ is adsorbed on a titania surface with Ti^{3+} defect sites, it reacts preferentially with these sites, becoming deprotonated, removing most of the oxygen radicals, and healing the defect sites.

Keywords: anatase · EPR spectroscopy · EXAFS spectroscopy · rhenium · surface chemistry

Introduction

Since the discovery of photocatalytic water splitting by titania electrodes,[1] the surface chemistry of titania has been investigated extensively, often with the goals of improved properties for photocatalytic reactions,[2,3] sensor applications, and applications as a support for catalytic groups.[4–6] Numerous investigations of titania surfaces have been carried out with single crystals under ultrahigh vacuum conditions, typically with samples lacking hydroxyl groups; some investigations have focused on the defect sites.[7] Henrich and Kurtz[8] showed that the dominant defect sites on the rutile (110) surface are oxygen vacancies (Ti^{3+} sites). Yamazaki et al.,[9] Park et al.,[10] and some of us[11] reported that an increase of the density of these surface defects can enhance the photoactivity by photoelectron trapping. Surface defects have also been inferred to play a significant role enhancing the dispersion of metals on high-area porous TiO_2.[4,5]

Surface defects can be created by treatment of rutile (110) (or anatase) under vacuum,[12–14] in H_2,[15] by ion bombardment,[16] or exposure to electron beams.[17] Electron-beam exposure can exclusively produce Ti^{3+} sites and less severe surface damage than results from ion bombardment,[17] which gives a variety of defects Ti^{n+} ($n=0$–3) and can produce high densities of defects. Vacuum treatment can also produce almost exclusively Ti^{3+} sites, which may be structurally more uniform than those produced by the other methods.[18] The vacuum treatment also does less structural damage to the titania surface than H_2 treatment or ion bombardment.[19]

[a] K. Suriye, R. J. Lobo-Lapidus, Prof. B. C. Gates
Department of Chemical Engineering and Materials Science
University of California, One Shields Ave., Davis, CA 95616 (USA)
Fax: (+1) 530-752-1031
E-mail: bcgates@ucdavis.edu

[b] K. Suriye, Prof. P. Praserthdam
Center of Excellence on Catalysis and Catalytic
Reaction Engineering, Department of Chemical Engineering
Chulalongkorn University, Bangkok 10330 (Thailand)

[c] G. J. Yeagle, Prof. R. D. Britt
Department of Chemistry, University of California
One Shields Ave., Davis, CA 95616 (USA)

Supporting information for this article is available on the WWW under http://www.chemeurj.org/ or from the author.

Titania surfaces incorporating Ti^{3+} sites can be monitored with techniques such as X-ray photoelectron spectroscopy,[20] ultraviolet photoelectron spectroscopy,[21] and electron paramagnetic resonance (EPR) spectroscopy.[22] Molecular probes have also been used to characterize defect sites on rutile (110) by thermal desorption (temperature-programmed desorption), with the probe molecules being O_2, which is photodesorbed,[12] and CO_2 and CO, which are thermally desorbed.[13,23] These methods distinguish Ti^{3+} from Ti^{4+} sites, for example.

The probe molecules O_2, CO and CO_2 that have been used to characterize rutile (110) are weakly bound to the defect sites, being desorbed at temperatures well below ambient. Although anatase is known to be more reactive and have higher surface areas than rutile for several photocatalytic applications,[2,3,9–11] there are still no reports of investigations of anatase surface defects with probe molecules. Our goal was to characterize the surface sites of anatase (prepared in a high-area porous form with surface hydroxyl groups) by a probe molecule of another class, one that would be rather strongly bound and offer spectroscopic signatures to help elucidate its interactions with the surface.

Thus, we chose a metal carbonyl with a relatively high molecular weight, $[Re_3(CO)_{12}H_3]$, because it offers the following potential advantages, assessed in the research described here:

- The ν_{CO} spectra are sensitive indicators of the bonding of $[Re_3(CO)_{12}H_3]$ to the surface.
- As $[Re_3(CO)_{12}H_3]$ is a proton donor, its reactions can provide evidence of the basic character of the surface sites on which it adsorbs.
- Extended X-ray absorption fine structure (EXAFS) spectra can be used to determine the bond lengths in the adsorbed probe molecule, giving evidence of its interaction with the surface.

Complementing the characterization methods listed in this paragraph, we also used infrared (IR) and EPR spectroscopies to characterize the surface species.

Results

X-ray diffraction characterization of titania before and after treatment: Hydroxylated, high-area porous powder titania (anatase) samples were prepared by a sol–gel method. Surface defect sites in titania samples were created as samples were treated at 723 K for 4 h in flowing O_2 (giving the sample referred to as TiO_{2ox}) or at 723 K for 4 h under vacuum (referred to as TiO_{2vac}).

X-ray diffraction (XRD) was used to characterize the as-prepared titania sample (designated simply as TiO_2) and the treated samples TiO_{2ox} and TiO_{2vac}. The XRD pattern of each sample (Figure 1) includes strong, sharp peaks at 25, 38, 48, 54, 55, 63, 69, 70, and 75°, matching that of anatase (JCPDS No. 21–1272).[24] The relative intensities of the various XRD peaks increased slightly as a result of the treatments, and each treatment gave essentially the same XRD pattern. Thus, we infer that 1) the small observed changes depend on the time of the treatment and not the atmosphere, 2) the bulk anatase structure was maintained in both treatments,[25] and 3) any significant changes resulting from the treatments were in the surface structure of the titania rather than the bulk.

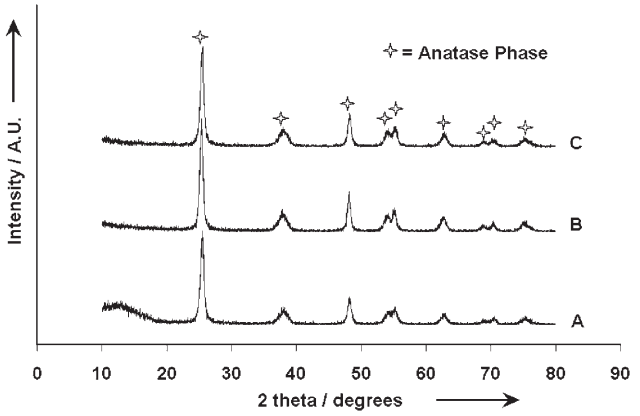

Figure 1. XRD patterns of titania samples: A) TiO_2, B) TiO_{2ox}, and C) TiO_{2vac}.

EPR evidence of radical species on titania before and after treatment: The EPR spectra of TiO_2, TiO_{2ox}, and TiO_{2vac} are shown in Figure 2. The spectrum of TiO_2 (Figure 2A) is in agreement with literature data[26–30] and essentially matches

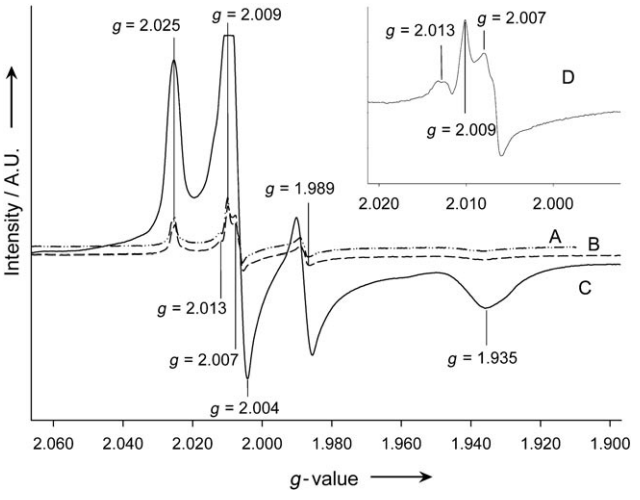

Figure 2. EPR spectra of titania samples: A) TiO_2 (offset for clarity), B) TiO_{2ox}, C) TiO_{2vac}, and D) another spectrum of TiO_{2vac} obtained by using a lower modulation amplitude and sweep width than were used to obtain spectrum C). Data for A)–C) were collected with frequency (ν_{MW}) = 9.68 GHz, modulation amplitude = 10 G, power = 2.00 mW, center field = 3400 G, sweep width = 1000 G, conversion time = 40.96 ms, time constant = 20.48 ms, and resolution = 2048 pts. Data for spectrum D) were collected with ν_{MW} = 9.68 GHz, modulation amplitude = 0.5 G, power = 2.00 mW, center field = 3400 G, sweep width = 450 G, conversion time = 80.48 ms, time constant = 40.96 ms, and resolution = 2048 pts, with an expected error in the g value of $\pm 6 \times 10^{-4}$.

that of TiO_{2ox} (Figure 2B). These spectra include signals in three groups, designated α, β, and γ, which are considered separately below and summarized in Table 1: α: $g_1=1.989$, $g_2=1.935$; β: $g_1=2.025$, $g_2=2.009$, $g_3=2.004$; γ: $g_1=2.013$, $g_2=2.007$.

Table 1. Results of EPR spectroscopy and comparison with literature: *g* values characterizing radicals formed on anatase surface.

Sample	Treatment	Environment[a]	Radical/ species	*g* value			Ref.
				g_1	g_2	g_3	
anatase	vacuum, 298 K	UV irradiation	Ti^{3+} (surface)	1.990		1.960	[26]
anatase	O_2, 973 K	UV irradiation	Ti^{3+} (surface)	1.990		1.957	[27]
Degussa P-25[b]	H_2, 773 K	–	Ti^{3+} (surface)	1.980		1.930	[28]
anatase	O_2, 723 K	vacuum	Ti^{3+} (surface)	1.989		1.935	this work
anatase	vacuum, 723 K	vacuum	Ti^{3+} (surface)	1.989		1.935	this work
anatase	hydration	vacuum	O_2^- (surface)[c]	2.025	2.009	2.003	[29]
anatase	–	O_2	O_2^- (surface)	2.024	2.009	2.003	[27]
anatase	O_2, 723 K	vacuum	O_2^- (surface)	2.025	2.009	2.004	this work
anatase	vacuum, 723 K	vacuum	O_2^- (surface)	2.025	2.009	2.004	this work
anatase	hydration	UV irradiation	O^- (surface)	2.016	2.012	2.002	[29]
TiO_2 colloid	–	water	O^- (surface)	2.014	2.007		[30]
anatase	O_2, 723 K	vacuum	O^- (surface)	2.013	2.007		this work
anatase	vacuum, 723 K	vacuum	O^- (surface)	2.013	2.007		this work

[a] During EPR measurement. [b] Mixture of anatase (75%) and rutile (25%). [c] From surface, not from O_2.

In contrast, the signals in the spectrum of the evacuated sample TiO_{2vac} are more intense (Figure 2C), as expected.[18,31,32] The strong features are classified into the same groups mentioned above (Table 1): α: $g_1=1.989$, $g_2=1.935$; and β: $g_1=2.025$, $g_2=2.009$, $g_3=2.004$. The signal at $g=2.009$ (Figure 2C) is clipped because of saturation of the detector diode under the collection conditions; thus, additional measurements were also made with a lower modulation amplitude and sweep width with greater values of the conversion time and time constant (Figure 2D), also allowing resolution of the flanking $g_2=2.013$ and $g_3=2.007$ about $g=2.009$ (Table 1). These resolved signals match those observed in the spectrum of TiO_2 prior to the vacuum treatment (Figure 2A).

The EPR results agree well with literature reports, as summarized in Table 1; typical errors in the *g* values are estimated to be $\pm 10^{-3}$ (unless stated otherwise). Thus, the signals in group α observed for all three samples ($g_1=1.989$, $g_2=1.935$) match within error those characterizing commercially available TiO_2 (P-25, Degussa, which consists of approximately 75% anatase and 25% rutile)[33] after H_2 treatment at 773 K.[28] These signals have been ascribed to Ti^{3+} surface-defect sites formed by removal of lattice oxygen.[28] They are also close to the signals attributed to Ti^{3+} sites that were observed for anatase treated under vacuum or in O_2 and characterized by EPR spectroscopy during UV irradiation.[26,27]

The signals of group β present in the spectra of each of the three samples ($g_1=2.025$, $g_2=2.009$, $g_3=2.004$) agree well with those found to represent O_2^- species on the anatase surface (Table 1).[26,29] The signals in group γ characteristic of each of the three samples ($g_1=2.013$, $g_2=2.007$) are very close to those found to represent O^- species on titania surfaces (Table 1).[29,30]

In summary, the EPR results agree well with the literature and show strong increases in the number of Ti^{3+} surface defects as well as O_2^- and O^- species as a result of the treatment under vacuum at 723 K.[31,32]

OH groups on titania before and after treatment: The IR spectra of TiO_2, TiO_{2ox}, and TiO_{2vac} are shown in Figure 3. The spectrum of TiO_2 essentially matches that of TiO_{2ox} (Figure 3A,B), including two strong peaks, at 3673 and 3716 cm^{-1}, and two shoulders, at 3640 and 3687 cm^{-1}. On the basis of the literature results summarized in Table 2, the peaks at 3673 and 3716 cm^{-1} are assigned to OH groups bonded to Ti^{4+} and to Ti^{3+}, respectively.[34–36] The

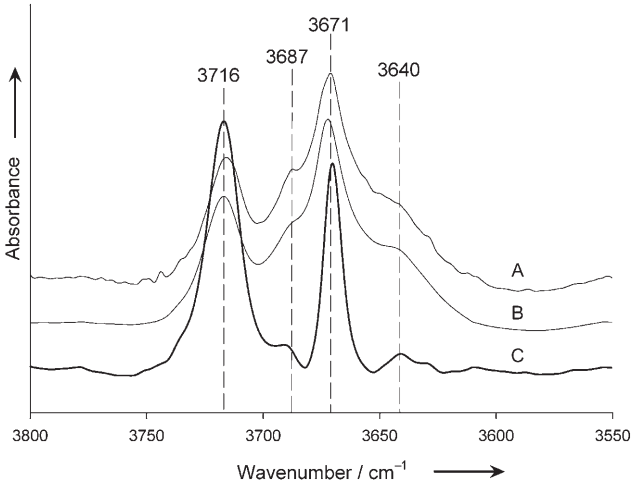

Figure 3. Normalized IR spectra in the ν_{OH} region characterizing titania samples: A) TiO_2, B) TiO_{2ox}, and C) TiO_{2vac}. Normalization was done by matching the heights of the peaks at approximately 3673 cm^{-1}.

shoulder at 3640 cm^{-1} is attributed to a bridging OH group $(Ti^{4+})_2$–OH.[36,37] The shoulder at 3687 cm^{-1} has been assigned to OH groups terminally bonded to Ti^{4+},[35] but we regard this assignment as less than firmly established.

The IR spectrum of TiO_{2vac} (Figure 3C) includes two strong peaks, at 3671 and 3716 cm^{-1}. To compare the areas of these bands, the spectra characterizing TiO_{2vac} and TiO_{2ox} were fitted by using a sum of Voigt-type lineshapes; relative areas and peak positions for each of the spectra are shown in Table 3 (plots of the fits are given in the Supporting Information). A comparison of the relative areas of the peaks at

Table 2. Infrared bands in the OH stretching region characterizing TiO_2.

Sample	Sample treatment	Environment[a]	ν_{OH} [cm^{-1}]	Species	Ref.
Degussa P-25[b]	UV irradiation	vacuum	3716	Ti^{3+}–OH^-	[34]
Degussa P-25[b]	partial deuteration	O_2	3716	Ti^{3+}–OH^-	[34]
anatase	O_2, 723 K	vacuum	3716	Ti^{3+}–OH^-	this work
anatase	vacuum, 723 K	vacuum	3716	Ti^{3+}–OH^-	this work
Degussa P-25[b]	UV irradiation	vacuum	approximately 3670	Ti^{4+}–OH	[34]
Degussa P-25[b]	partial deuteration	O_2	approximately 3670	Ti^{4+}–OH	[34]
anatase	NH_3, 373–873 K	–	3685–3700	Ti^{4+}–OH	[35]
anatase	–	–	3670	Ti^{4+}–OH	[36]
anatase	O_2, 723 K	vacuum	3687, 3673	Ti^{4+}–OH	this work
anatase	vacuum, 723 K	vacuum	3687, 3671	Ti^{4+}–OH	this work
anatase	–	–	3640	$(Ti^{4+})_2$–OH	[36]
Degussa P-25[b]	–	pyridine	3640	$(Ti^{4+})_2$–OH	[37]
anatase	O_2, 723 K	vacuum	3640	$(Ti^{4+})_2$–OH	this work
anatase	vacuum, 723 K	vacuum	3640	$(Ti^{4+})_2$–OH	this work

[a] During IR measurement. [b] Mixture of anatase (75%) and rutile (25%).

Table 3. Relative peak areas determined by integration from fitting of IR spectra characterizing TiO_{2vac} and TiO_{2ox} samples.[a]

Sample	Peak at 3671 cm^{-1}	Peak at 3716 cm^{-1}	Peak at 3640 cm^{-1}	Peak at 3687 cm^{-1}
TiO_{2vac}	1	2.59	0.08	0.06
TiO_{2ox}	1	0.81	0.74[b]	0.49[c]

[a] Voigt line shapes were used to fit all the spectra. [b] Position of this peak (3646 cm^{-1}) is not reliable because of low integrated area (<2% of the total area). [c] Position of this peak (3687 cm^{-1}) not reliable because of low integrated area (<2% of the total area).

3671 and 3716 cm^{-1} shows that the treatment under vacuum led to a strong increase in relative area of the band at 3716 cm^{-1} relative to that at 3671 cm^{-1}, indicating a strong increase in the number of Ti^{3+}–OH groups relative to Ti^{4+}–OH groups. This treatment also led to the removal of bridging OH groups, indicated by the strong decrease in intensity of the peak at 3640 cm^{-1} (Figure 3C) as well as a strong increase in intensity of the EPR signals characterizing Ti^{3+} surface-defect sites (Figure 2).

Rhenium carbonyls formed from $[Re_3(CO)_{12}H_3]$ on treated titania: $[Re_3(CO)_{12}H_3]$ in solution with *n*-pentane was allowed to react with samples of the treated titania powder (TiO_{2ox} and TiO_{2vac}). After removal of the solvent, two of these samples contained 1.00 ± 0.04 wt% Re loading, and a sample made similarly from TiO_{2vac} was brought in contact with a smaller amount of $[Re_3(CO)_{12}H_3]$, giving a sample with a 0.10 ± 0.04 wt% loading of Re.

IR spectra characterizing the ν_{CO} region of 1) $[Re_3(CO)_{12}H_3]$ in CH_2Cl_2, and samples formed from $[Re_3(CO)_{12}H_3]$ containing 2) 1 wt% Re on TiO_{2ox}, 3) 1 wt% Re on TiO_{2vac}, and 4) 0.1 wt% Re on TiO_{2vac} are shown in Figure 4A–D, respectively. The ν_{CO} IR spectrum characterizing $[Re_3(CO)_{12}H_3]$ in CH_2Cl_2 (Figure 4A) includes strong peaks at 2095, 2031, 2007, and 1977 cm^{-1}, representing carbonyl groups bonded to the triangular rhenium frame.[38,39] The spectra characterizing the species formed from $[Re_3(CO)_{12}H_3]$ on TiO_{2ox} and TiO_{2vac} are similar, but with broadened and shifted ν_{CO} peaks, consistent with the results of Kirlin et al.[39] for species formed from $[Re_3(CO)_{12}H_3]$ adsorbed on γ-Al_2O_3 and on MgO. The peak broadening is attributed to the intrinsic nonuniformity of the surfaces and the consequent variations in adsorbate structure.[40] A summary of the IR absorption bands of rhenium carbonyls on various supports is given in Table 4.

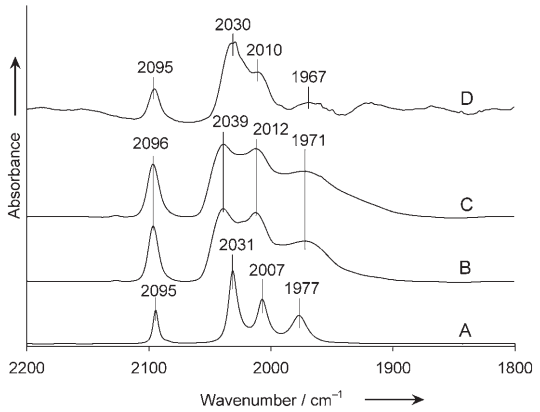

Figure 4. Normalized IR spectra in the ν_{CO} region characterizing: A) $[Re_3(CO)_{12}H_3]$ in CH_2Cl_2, B) sample containing 1 wt% Re on TiO_{2ox} formed from $[Re_3(CO)_{12}H_3]$; C) sample containing 1 wt% Re on TiO_{2vac} formed from $[Re_3(CO)_{12}H_3]$; and D) sample containing 0.1 wt% Re on TiO_{2vac} formed from $[Re_3(CO)_{12}H_3]$. Normalization was done by matching the heights of the peak at approximately 2031 cm^{-1}.

Table 4. CO stretching frequencies of adsorbed rhenium carbonyls formed from $[Re_3(CO)_{12}H_3]$ and various supports.

Loading [wt%][a]	Surface/treatment	ν_{CO} bands[b] [cm^{-1}]	Ref.
1	TiO_2/O_2 at 723 K	2096 (s), 2039 (m), 2012 (m), 1971 (mw)	this work
1	TiO_2/vacuum at 723 K	2096 (s), 2039 (m), 2012 (m), 1970 (mw)	this work
0.1	TiO_2/vacuum at 723 K	2095 (s), 2030 (m), 2010 (m), 1967 (mw)	this work
1.3	γ-Al_2O_3	2098 (m), 2032 (b), 2013 (b), 1966 (sh)	[39]
2.2	MgO	2096 (s), 2000 (s), 1978 (s), 1872(s)	[39]

[a] Loading of the Re in the sample. [b] The ν_{CO} bands characterizing $[Re_3(CO)_{12}H_3]$ in a dichloromethane solution are 2095 (s), 2031 (s), 2007 (s), and 1977 (sm), which agree well with those reported,[38] namely, 2096 (s), 2035 (s), 2012 (s), and 1979 (s). The symbols (s), (m), (mw), (b), and (sh) stand for strong, medium, weak, broad, and shoulder, respectively.

The ν_{CO} IR spectra characterizing the TiO_{2vac} samples incorporating $[Re_3(CO)_{12}H_3]$ with 1 and 0.1 wt% Re loadings (Figure 4C,D) show the same IR features.[41]

OH groups on treated titania with adsorbed rhenium carbonyls: There was no influence of remnants of the *n*-pentane used in the sample preparation on the IR spectra characterizing either of the treated titania samples, TiO_{2ox} and TiO_{2vac} (Supporting Information), but adsorption of rhenium carbonyls led to changes in the IR spectra of the titania.

The ν_{OH} IR spectrum characterizing the TiO_{2ox} incorporating adsorbed rhenium carbonyls with a 1 wt% Re loading (Figure 5A) shows the same features as the sample with

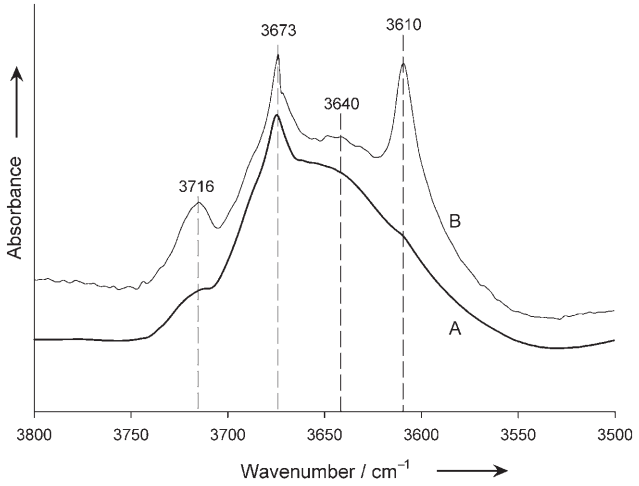

Figure 5. Normalized IR spectra in the ν_{OH} region of the samples formed by adsorption of $[Re_3(CO)_{12}H_3]$ (1 wt% Re) on A) TiO_{2ox} and B) TiO_{2vac}. Normalization was done by matching the heights of the peaks at approximately 3671 cm^{-1}.

clusters adsorbed on TiO_{2vac} at the same surface concentration (Figure 5B). Adsorption of $[Re_3(CO)_{12}H_3]$ caused the peak at 3716 cm^{-1} to decrease strongly in intensity relative to that at 3673 cm^{-1}, accompanied by an increase in intensity of the shoulder at 3640 cm^{-1}. These results indicate that adsorption of $[Re_3(CO)_{12}H_3]$ led to the removal of terminally bonded OH groups at Ti^{3+} sites and the formation of bridging OH groups.

When $[Re_3(CO)_{12}H_3]$ was adsorbed on TiO_{2vac} at a loading of 1 wt% Re, a new IR peak was observed at 3610 cm^{-1} (Figure 5).[42]

To test the inference that the decrease in the number of OH groups bonded to Ti^{3+} was associated with the increase in the number of bridging OH groups, the surface concentration of rhenium carbonyls on TiO_{2vac} was varied; the same behavior regarding the changes in these bands was observed at several different Re loadings (Figure 6).

EPR evidence of radical species on treated titania with adsorbed rhenium carbonyls: There was no influence of *n*-pentane on the EPR signals characterizing either of the treated

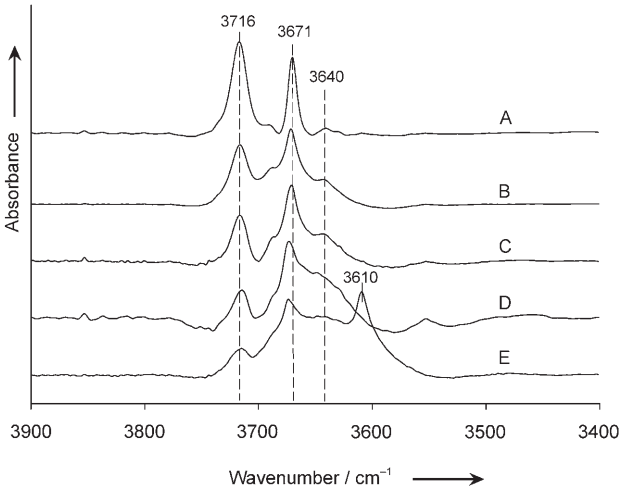

Figure 6. Normalized IR spectra in the ν_{OH} region characterizing samples formed by adsorption of $[Re_3(CO)_{12}H_3]$ on TiO_{2vac} with various Re contents (wt%): A) 0, B) 0.1, C) 0.3, D) 0.6, and E) 1. Normalization was done by matching the heights of the peak at approximately 3673 cm^{-1}.

titania samples, TiO_{2ox} and TiO_{2vac} (Supporting Information), but adsorption of rhenium carbonyls led to changes in the EPR spectra. Adsorption of $[Re_3(CO)_{12}H_3]$ on the sample treated in O_2 (TiO_{2ox}) (1 wt% Re) led to the disappearance of the EPR signals characterizing Ti^{3+}, O_2^-, and O^- (Figure 7A). A comparison with the spectrum of the sample prior to adsorption of the rhenium carbonyl (Figure 7B) shows that the $[Re_3(CO)_{12}H_3]$ saturated (quenched) the Ti^{3+} surface-defect sites.

The integrated area of the EPR spectrum of the TiO_{2vac} sample and that of the TiO_{2vac} sample containing 1 wt% Re

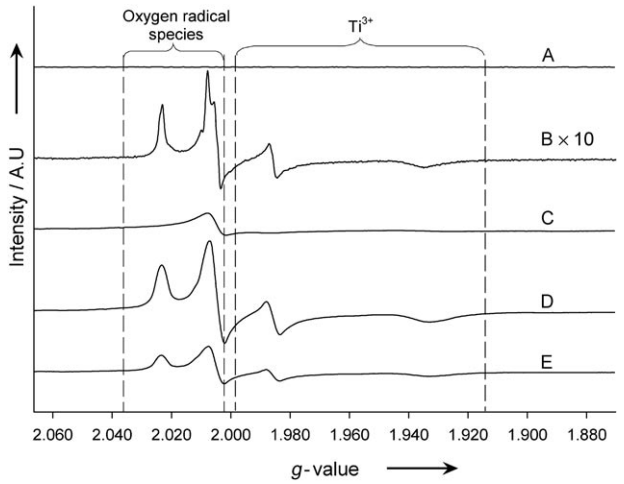

Figure 7. EPR spectra of titania and samples formed by adsorption of $[Re_3(CO)_{12}H_3]$ on titania: A) 1 wt% Re on TiO_{2ox}, B) TiO_{2ox} (spectrum multiplied by a factor of 10 for clarity), C) 1 wt% Re on TiO_{2vac}, D) TiO_{2vac}, and E) 0.1 wt% Re on TiO_{2vac}. Data were collected with frequency (ν_{MW}) = 9.68 GHz, modulation amplitude = 10 G, power = 2.02 mW, center field = 3450 G, sweep width = 1200 G, conversion time = 40.96 ms, time constant = 20.48 ms, and resolution = 2048 pts.

(Figure 7C) were used for a rough comparison of the amounts of Ti^{3+} initially present and that present after adsorption of the rhenium carbonyl. The adsorption led to a reduction of the signals at $g=1.989$ and 1.935 to roughly 8 and 2%, respectively, of that characteristic of TiO_{2vac}, although the latter value is not distinguishable from 0 within the error in the data. Thus, we infer that the adsorbed species completely removed all or almost all of the Ti^{3+} sites on TiO_{2vac}; this behavior matches that observed with TiO_{2ox}. A comparison of the spectrum with that of TiO_{2vac} without adsorbed rhenium carbonyls (Figure 7D) shows that the signals at $g=2.004$ and 2.009 had been significantly reduced in intensity as a result of the adsorption and that the signal at $g=2.024$ was completely removed. A comparison of the total area of the peaks before and after adsorption of the rhenium carbonyls showed that this area was reduced to about 30% of that of TiO_{2vac}. Taken together, these results imply that the removal of the O_2^- and O^- species from TiO_{2vac} was incomplete at a Re loading of 1 wt%, in contrast to the observations with the TiO_{2ox} sample containing 1 wt% Re.

Figure 7E,C shows the EPR spectra of the TiO_{2vac} sample incorporating the lower and higher loadings of rhenium carbonyls (0.1 and 1 wt% Re, respectively). A comparison of the integrated area of former spectrum with that of TiO_{2vac} without rhenium (Figure 7D) shows the peaks at $g=1.935$ and 1.989 were reduced to 37 and 32% of those characteristic of TiO_{2vac}, respectively. Thus, the data show that the Ti^{3+} surface-defect sites reacted with—but were not saturated by—the rhenium carbonyls at the lower surface concentration. Correspondingly, the EPR signals indicating oxygen radical species were also observed for the sample containing 0.1 wt% Re (Figure 7E).

EXAFS data characterizing rhenium carbonyls on treated titania: In the EXAFS analysis, it was found that two models gave good fits to the experimental results characterizing each of the samples incorporating adsorbed rhenium carbonyls, and much better fits than any other that made physical sense. Each successful fit included the following contributions: Re–Re, Re–C, and Re–O, the last being characterized by multiple scattering. The two fits differ in that one includes a Re–O contribution at a longer-than-bonding length, whereas the other includes a Re–Ti contribution instead. We proceed with these two fits.

The results corresponding to the best fit for each sample according to each model are summarized in Tables 5–7, together with errors (precisions, not accuracies) estimated with XDAP.[47] Representative plots of the data and the fits in *k*- and *R*-space for the sample containing 1 wt% Re on TiO_{2vac} according to the model including a Re–O contribution at a longer-than-bonding length are shown in Figure 8; plots for the other samples and models are given in Supporting Information.

Sample incorporating 1 wt% Re on TiO_{2ox} (Table 5): The model representing the sample containing 1 wt% Re on TiO_{2ox} includes a Re–Re contribution with a coordination number of nearly two at distances of 2.98 Å for one model (designated model A) and 2.97 Å for another (designated model B). The coordination number indicates that the trirhenium frame remained essentially intact upon adsorption

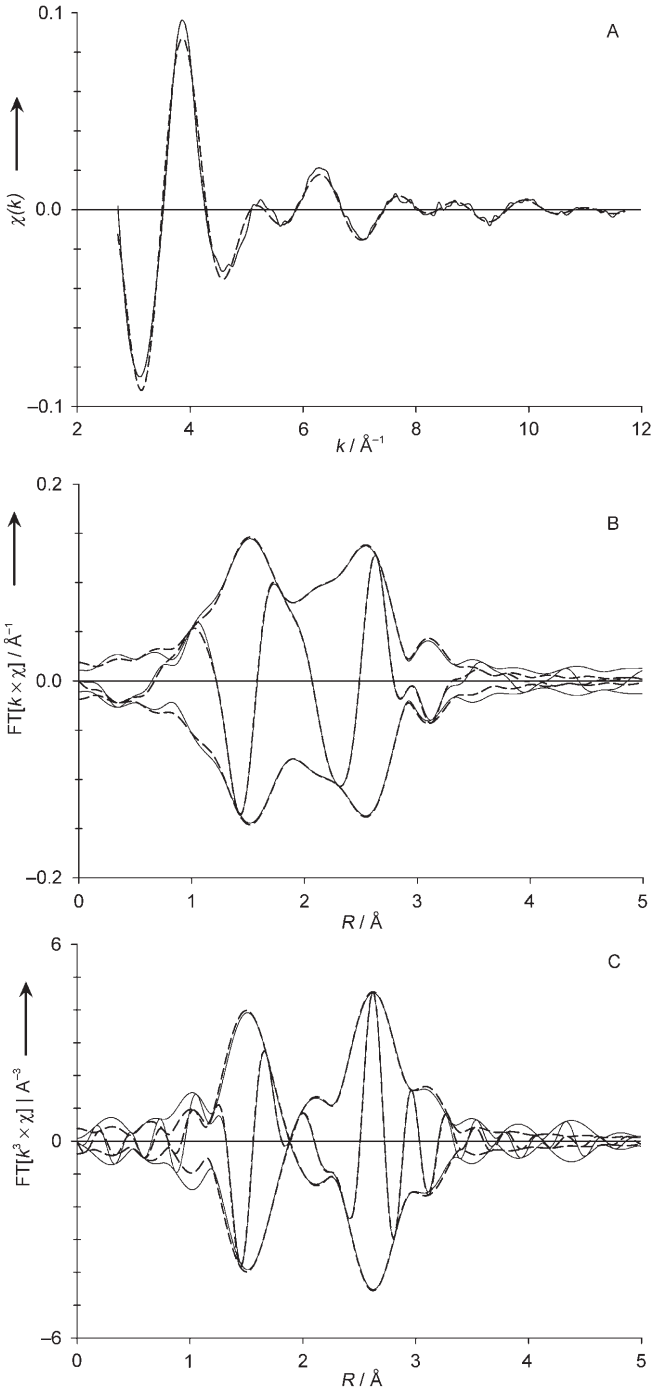

Figure 8. EXAFS data characterizing sample formed from $[Re_3(CO)_{12}H_3]$ and TiO_{2vac} containing 1 wt% Re. Experimental results, continuous line; fit (model) including Re–O contribution at $R=2.57$ Å, broken line. A) k^0-weighted EXAFS function in *k*-space, B) imaginary part and magnitude of k^1-weighted EXAFS function in *R*-space, and C) imaginary part and magnitude of k^3-weighted EXAFS function in *R*-space.

Table 5. EXAFS results characterizing sample containing 1 wt% Re on TiO_{2ox}.[a]

Absorber–backscatterer pair	N	R [Å]	$\Delta\sigma^2\times10^3$ [Å^2]	ΔE_0 [eV]
Model A: goodness of fit = 46 $(\Delta\chi)^2 = 97$				
Re–C	3.9±0.0	1.93±0.00	3.2±0.1	−3.7±0.0
Re–O[b]	4.3±0.0	3.10±0.00	4.1±0.2	−0.7±0.0
Re–Re	2.5±0.1	2.98±0.01	7.4±0.8	−4.7±0.2
Re–Ti	0.5±0.0	2.66±0.01	3.9±0.9	−8.3±0.4
Model B: goodness of fit = 42 $(\Delta\chi)^2 = 75$				
Re–C	4.1±0.0	1.93±0.00	3.5±0.2	−3.6±0.1
Re–O[b]	4.2±0.0	3.10±0.00	4.1±0.3	0.4±0.1
Re–Re	2.4±0.1	2.97±0.01	7.3±0.6	−4.5±0.3
Re–O	1.5±0.0	2.59±0.01	4.7±1.0	−9.8±0.3

[a] Notation: N, coordination number; R, distance between absorber and backscatterer atoms; $\Delta\sigma^2$, Debye–Waller factor relative to reference material; and ΔE_0, inner potential correction. The mean free path was taken as 6 Å. The k- and R-ranges were 2.71–11.74 Å^{-1} and 0.5–4.0 Å, respectively. The number of independent points for the calculation with the Nyquist theorem was 22. All intervals reported in this table correspond to precisions associated with the fit. The accuracies associated with the model parameters are, for the metal-metal shell: N: ±10%, R: ±0.02 Å, $\Delta\sigma^2$: ±20%, ΔE_0: ±20%; and for the metal-light scatterer shells: N: ±20%; R: ±0.02 Å; $\Delta\sigma^2$: ±20%; ΔE_0: ±20%. [b] The Re–O contribution is characterized by co-linear multiple scattering in the group Re-C-O.

Table 6. EXAFS results characterizing sample containing 1 wt% Re on TiO_{2vac}.[a]

Absorber–backscatterer pair	N	R [Å]	$\Delta\sigma^2\times10^3$ [Å^2]	ΔE_0 [eV]
Model A: goodness of fit = 34 $(\Delta\chi)^2 = 42$				
Re–C	3.6±0.0	1.95±0.00	3.2±0.1	−4.8±0.0
Re–O[b]	4.5±0.0	3.09±0.00	4.9±0.1	0.0±0.0
Re–Re	1.7±0.1	2.93±0.00	3.0±0.3	11.1±0.5
Re–Ti	0.4±0.0	2.62±0.01	5.9±1.0	1.3±0.6
Model B: goodness of fit = 20 $(\Delta\chi)^2 = 22$				
Re–C	3.7±0.0	1.95±0.00	3.2±0.1	−4.7±0.0
Re–O[b]	4.3±0.0	3.13±0.00	6.4±0.1	−0.8±0.0
Re–Re	2.3±0.1	2.94±0.00	5.0±0.4	−3.8±0.2
Re–O	1.4±0.0	2.57±0.00	7.5±0.6	−8.2±0.1

[a] See Footnote [a] in Table 5. The k and R ranges were 2.72–11.74 Å^{-1} and 0.5–4.0 Å^{-1}, respectively. The number of independent points was 22. [b] The Re–O contribution was characterized by co-linear multiple scattering in the group Re-C-O.

of the clusters. The Re–Re distance in the adsorbed clusters is significantly shorter than that in crystalline $[Re_3(CO)_{12}H_3]$ (3.28 Å) and closer to those in the anion $[Re_3(CO)_{12}H]^{2-}$ (3.02 and 3.13 Å[48]). The comparison suggests that the rhenium carbonyls were deprotonated upon adsorption on TiO_{2ox}, consistent with the basicity of the surface.[49]

The Re–C and Re–O contributions in each model are characterized by multiple scattering (as expected for linear Re–C–O moieties), with Re–C and Re–O distances of 1.93 and 3.10 Å, respectively, consistent with carbonyl ligands bonded to rhenium.[50] The Re–C and Re–O coordination number found for each model (approximately 4) corresponds to the Re:CO ratio of the precursor $[Re_3(CO)_{12}H_3]$ and indicates the lack of decarbonylation of the clusters upon adsorption, consistent with the ν_{CO} spectra.

The key difference between the two models is that model A includes a Re–Ti contribution, and Model B instead includes a Re–O contribution other than the Re–carbonyl-oxygen contribution; the respective Re–Ti and Re–O distances are 2.66 and at 2.59 Å, and the respective coordination numbers are 0.5 and 1.5. The coordination number and length of the Re–O contribution in the latter model are in agreement with other observations;[51] they would be expected to depend on the surface-site geometry and possible distortion of the carbonyl ligands on the cluster. The parameters characterizing the Re–Ti contribution in the former model are also plausible. The goodness of fit is better for the model containing the Re–O contribution-and the value of $(\Delta\chi)^2$ is smaller, and thus we prefer this model.

Sample incorporating 1 wt% Re on TiO_{2vac} (Table 6): As for the sample containing 1% Re on TiO_{2ox}, the two models representing the EXAFS data characterizing the sample that had been treated in vacuum each incorporate a Re–Re contribution with a coordination number of two, within error, at a distance of 2.93 Å for model A and 2.94 Å for model B; these are significantly shorter than the distance observed for $[Re_3(CO)_{12}H_3]$ (3.24 Å).[50] As for the sample prepared from TiO_{2ox}, this distance agrees better with a Re–Re distance characteristic of deprotonated clusters than of $[Re_3(CO)_{12}H_3]$.[50]

Again, as for the sample containing 1 wt% Re on TiO_{2ox}, the EXAFS data indicate the presence of carbonyl ligands (a Re–C and a Re–O contribution characterized by multiple scattering) with a coordination number of approximately four, at distances of 1.95 and 3.09 Å for model A and 1.95 and 3.13 Å for model B, respectively, consistent with the inference that the rhenium clusters were not substantially decarbonylated upon adsorption, and in agreement with observations of adsorption of $[Re_3(CO)_{12}H_3]$ on other metal oxides.[39]

The distances of the Re–Ti and Re–O contributions in the two models are 2.62 and 2.57 Å, and the respective coordination numbers are 0.4 and 1.4. These parameters match those observed for the sample containing 1 wt% Re on TiO_{2ox}, and the model including the Re–O contribution gave a far better fit than the one with a Re–Ti contribution, as judged by the goodness of fit and the value of $(\Delta\chi)^2$ (which are 33 and 48% lower, respectively, for the model with the Re–O contribution than for the other).

Sample incorporating 0.1 wt% Re on TiO_{2vac} (Table 7): The quality of the EXAFS data characterizing the sample with the low Re content (0.1 wt%) on TiO_{2vac} is lower than that of the other samples, but of sufficient quality for a satisfactory data analysis. The goodness of fit and $(\Delta\chi)^2$ criteria do not provide a basis for distinguishing between the two models (Table 7). We tentatively prefer the model incorporating the Re–O rather than the Re–Ti contribution on the basis of an assumed analogy with the samples with the higher rhenium loading.

Table 7. EXAFS results characterizing 0.1 % Re on TiO_{2vac}.[a]

Absorber–backscatterer pair	N	R [Å]	$\Delta\sigma^2\times10^3$ [Å^2]	ΔE_0 [eV]
Model A: goodness of fit = 11 $(\Delta\chi)^2=29$				
Re–C	3.9 ± 0.0	1.81 ± 0.00	7.8 ± 0.0	0.6 ± 0.1
Re–O[b]	4.2 ± 0.0	3.11 ± 0.00	11.0 ± 0.3	−1.1 ± 0.0
Re–Re	2.3 ± 0.1	2.90 ± 0.00	4.2 ± 0.6	0.8 ± 0.3
Re–Ti	0.7 ± 0.0	2.60 ± 0.01	5.9 ± 1.0	−8.8 ± 0.4
Model B: goodness of fit = 11 $(\Delta\chi)^2=30$				
Re–C	4.0 ± 0.0	1.81 ± 0.00	8.1 ± 0.2	1.1 ± 0.1
Re–O[b]	3.9 ± 0.0	3.13 ± 0.00	11.5 ± 0.3	−1.6 ± 0.1
Re–Re	2.2 ± 0.1	2.86 ± 0.00	2.2 ± 0.5	9.6 ± 0.3
Re–O	1.4 ± 0.0	2.49 ± 0.00	7.3 ± 0.9	−1.1 ± 0.2

[a] See Footnote [a] in Table 5. The k- and R-ranges were 2.68–10.42 Å and 0.5–4.0 Å, respectively. The number of independent points was 19. [b] The Re-O contribution was characterized by co-linear multiple scattering of the group Re-C-O.

As for the samples containing 1 wt % Re, both of the models providing a good fit include a Re–Re contribution with a coordination number of nearly two. However, the models apparently differ slightly from each other in that the Re–Re distances are 2.86 and 2.90 Å for the models including the Re–O and Re–Ti contributions, respectively (but we emphasize that the calculated differences are within the uncertainty of the Re–Re distances).

According to the model including the Re–O contribution, this distance is significantly shorter than that observed for the samples containing 1 % Re on either TiO_{2vac} or TiO_{2ox}. This result suggests that the Re–Re bond was strengthened upon adsorption of the cluster at the low loading (at the Ti^{3+} defect site). In the model with the Re–Ti contribution, the differences between the parameters and those characterizing the sample incorporating 1 wt % Re are too small to resolve.

In both models of the sample containing 0.1 wt % Re, Re–C and Re–O contributions characterized by multiple scattering were observed, with a coordination number of four for each shell, and distances of 3.11 and 3.13 Å for models A and B, respectively, for the Re–O contribution, matching that observed for the samples containing 1 wt % Re. In contrast, a Re–C distance of 1.81 Å was observed for both models characterizing the sample containing only 0.1 % Re on TiO_{2vac}; this distance is more than 0.12 Å shorter than that found for the samples containing 1 wt % Re on either titania sample. This comparison suggests that the Re–C bonds were stronger in the former sample than in the latter. Furthermore, this distance is closer to that observed[48] for $[Re_3(CO)_{12}H]^{2-}$, which suggests that a greater degree of cluster deprotonation was achieved in this sample, in which the clusters were bonded at Ti^{3+} defect sites.

According to the fit for the model including a Re–Ti contribution, this contribution is characterized by a coordination number of 0.7 at a distance of 2.60 Å. These values match, within error, those determined for the two samples containing 1 wt % Re for the same model.

According to the fit for the model including a Re–O contribution, this contribution is characterized by a coordination number of 1.4 at a distance of 2.49 Å. The latter value is significantly shorter than that observed for the two samples containing 1 wt % Re and therefore indicates a stronger interaction of the metal clusters with the support in the sample with the low rhenium loading than in the samples with the high rhenium loading.

In summary, according to either model, a strong interaction of the clusters with the support is indicated, and in the model with the Re–O and not the Re–Ti contribution the data distinguish a stronger cluster-support interaction than for the samples containing 1 wt % Re.

Discussion

Formation of defect sites on titania: The data reported here are consistent with the literature[18,31,32] in demonstrating that treatment of titania under vacuum at 723 K leads to the formation of defects identified as Ti^{3+} at oxygen vacancy sites on the surface (Figures 2 and 3). Formation of a surface-defect site has been explained as the result of removing a lattice oxygen atom and one electron during the treatment, with one electron being left in the d orbital of the neighboring surface Ti site,[12,13,26] resulting in the reduction of Ti^{4+} to Ti^{3+}.

The IR spectra show that surface Ti^{3+}–OH groups were formed as bridging OH groups were removed (Figure 3), generating surface-defect sites and oxygen radical species (as demonstrated by EPR spectroscopy, Figure 2). These results are the first demonstration that formation of defect sites and oxygen radicals on titania is accompanied by the disappearance of bridging OH groups and the formation of OH groups associated with the defect sites.

The increase in the number of surface-defect sites during the vacuum treatment (as evidenced by the IR and EPR spectra)—but not during the O_2 treatment—implies that residual oxygen in the system or readsorption of oxygen were not responsible for the formation of the defect sites and the radical species associated with them.

Thus, the results show how EPR and IR spectroscopy complement each other as methods for characterization of titania surface chemistry. The use of a metal carbonyl as a surface probe also goes beyond what has been reported, as discussed below.

There are two types of lattice oxygen on the most stable (1 1 0) single-crystal rutile surface, that is, bridging and in-plane lattice oxygen.[12,53] STM images show that the two-fold-coordinated bridging lattice oxygen is removed more easily than the threefold-coordinated in-plane lattice oxygen,[54] and removal of the former can even eliminate entire rows of rutile oxygen atoms during treatment under vacuum.[55]

There is a lack of such information for anatase, but, on the basis of the aforementioned STM results and the fact that the predominant face of anatase is the (1 0 1)[56–59] [which is similar to the (1 1 0) face of rutile-having the same five- and sixfold coordinated Ti atoms and the same two-

and threefold coordinated oxygen atoms, but at different angles], we suggest that the formation of surface-defect sites (Ti^{3+}) on our TiO_{2vac} (anatase) sample likely resulted from the removal of bridging lattice oxygen atoms. This suggestion is consistent with both IR spectra, showing the removal of bridging OH groups as defect sites are formed, and theoretical results,[58,60] showing how water adsorbs on the (101) face of anatase after removal of bridging oxygen atoms.

The EPR data show that, after removal of lattice oxygen, some oxygen remained on the titania surface in the form of either O_2^- or O^- (Figure 2). Because no increase in the intensity of the EPR peaks indicative of O_2^- and O^- was observed when the sample was treated in O_2 (to prepare TiO_{2ox}), we infer that these radical species did not form from O_2, but instead from lattice oxygen, as has been suggested by Howe et al.[29]

Carter et al.[61] published results dealing with EPR characterization of the O_2^- radicals on the anatase phase of Degussa P-25; samples were treated under oxygen (resulting in samples with no EPR signals), and then under vacuum at 573 and at 723 K. The EPR spectra characterizing these samples contain only signals representing Ti^{3+} species. Exposure to oxygen led to the removal of such signals and the appearance of O_2^- signals. These results are significantly different from what is reported in this paper, whereas the appearance of Ti^{3+} species (evident in the EPR and IR spectra) and O_2^- radicals (observed by EPR spectroscopy) was observed in a vacuum-treated sample without exposure to oxygen. Furthermore, we observed evidence of the presence of Ti^{3+} sites (by IR and EPR spectroscopy) and O_2^- radicals in samples treated under oxygen at 723 K, treatments that Carter et al. claim to yield no EPR signal. Moreover, the fact that all the EPR signals (both for Ti^{3+} and oxygen radicals) characterizing TiO_{2vac} samples were substantially more intense than those characterizing the TiO_{2ox} sample suggests that O_2 is not required for the creation of the radical species.

Schematic representation of formation of defects on titania surface: On the basis of the EPR and IR results, we propose a simplified representation (Figure 9) to explain the changes in the anatase surface resulting from treatment under vacuum. This model is proposed for the predominant anatase (101) surface.

As shown in Figure 9, the surface of untreated titania incorporates relatively few Ti^{3+} sites and O_2^- and O^- species as shown by the relatively low-intensity EPR signals. This surface also incorporates a low density of Ti^{3+}–OH groups ($\nu_{OH}=3716\ cm^{-1}$) and a relatively high density of bridging OH groups ($\nu_{OH}=3643\ cm^{-1}$) (Figure 3).

Treatment of this sample under vacuum (giving TiO_{2vac}) led to an increase in the number of Ti^{3+} sites ($g=1.989$ and 1.935, Figure 2C) and O^- species ($g=2.013$ and 2.007, Figure 2C) and a simultaneous increase in the number of Ti^{3+}–OH groups ($\nu_{OH}=3716\ cm^{-1}$, Figure 3C). We postulate that these changes are initiated on Ti^{4+} sites incorporating OH groups (as the bond between a bridging lattice oxygen and a

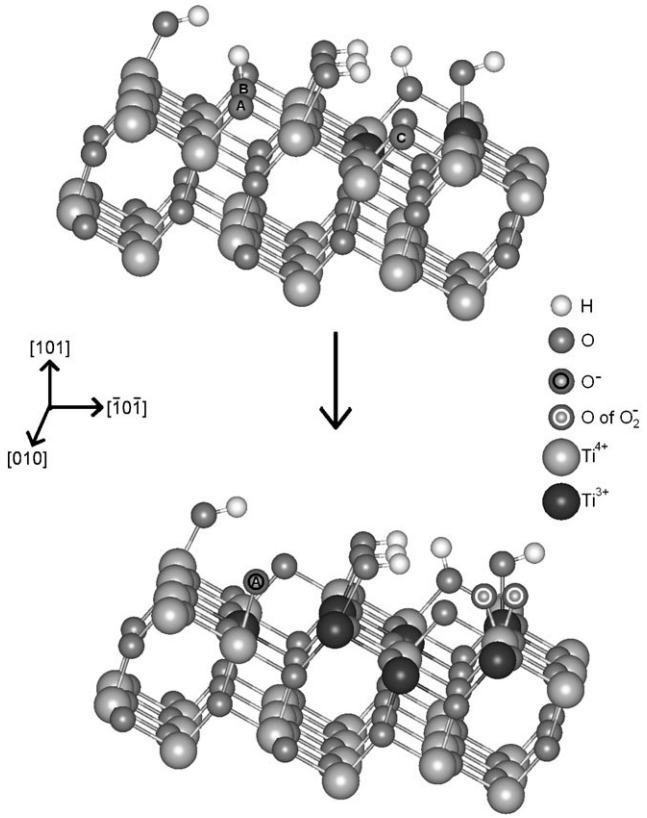

Figure 9. Representation of the hydroxylated anatase (101) surface before and after treatments, as characterized by EPR and IR spectroscopy. A) Bridging oxygen group that upon treatment becomes a Ti^{4+}–O^- species and leaves a Ti^{3+} site; B) bridging hydroxyl group that is removed upon treatment, leaving behind two Ti^{3+} sites; and C) bridging oxygen that is removed upon treatment, leaving behind two Ti^{3+} sites.

Ti^{4+} ion is broken), an O^- species is formed, leading to the reduction of a Ti^{4+} to a Ti^{3+} site and correspondingly of Ti^{4+}–OH into Ti^{3+}–OH groups (Figure 9A).

Treatment of titania under vacuum also led to a decrease in the number of bridging OH groups ($\nu_{OH}=3640\ cm^{-1}$) and a simultaneous increase in the number of Ti^{3+}–OH groups ($\nu_{OH}=3716\ cm^{-1}$) (Figure 3). We postulate that these changes resulted from removal of bridging OH groups and the simultaneous conversion of Ti^{4+}–OH into Ti^{3+}–OH groups (Figure 9B). We also infer that formation of O_2^- species characterized by EPR spectroscopy (Figure 2C, $g=$ 2.025, 2.009, and 2.004) resulted from removal of bridging lattice oxygen atoms (Figure 9C), but the mechanism of this reaction remains unclear.[62]

In summary, the simplified representation shown in Figure 9 is consistent with both the EPR and IR data and explains the formation of surface Ti^{3+} defect sites; it is broadly consistent with the literature and specifically with the more restricted representation of Tilocca and Selloni,[60] which however does not involve OH groups in the formation of defect sites. Their representation instead accounts for OH groups resulting from the dissociation of water on

the defect sites-and experimental evidence of such OH group formation has been presented by Henderson.[49]

Probing titania defect sites with rhenium carbonyl clusters: Both TiO_{2vac} and TiO_{2ox} lost Ti^{3+} surface-defect sites ($g=$ 1.989 and 1.935) when the rhenium carbonyl was adsorbed, as demonstrated by the EPR spectra (Figure 7). This change was accompanied by a decrease in the density of Ti^{3+}–OH groups (3716 cm^{-1}, Figure 5). These results might be explained by either of two mechanisms: 1) rhenium carbonyl clusters became bonded to Ti^{3+} sites and accepted lone-pair electrons from d orbitals of Ti^{3+}, leading to the formation of Re–Ti bonds or 2) rhenium carbonyl clusters healed the surface defects (Ti^{3+}) at oxygen vacancy sites, oxidizing Ti^{3+} to Ti^{4+} sites.

The IR results (Figure 5) show that, after adsorption of $[Re_3(CO)_{12}H_3]$, especially on TiO_{2vac}, the bridging OH groups became evident and the density of the Ti^{3+}–OH groups and surface-defect sites (Ti^{3+}) decreased (Figure 6), consistent with the suggestion of a process of healing of the defect sites by the rhenium carbonyls. Thus, the data show how the rhenium carbonyl is an informative probe of the chemistry of the Ti^{3+} surface-defect sites.

The IR and EPR spectra are both sensitive to the loading of rhenium carbonyls on the surface (Figures 6 and 7). When the loading of Re on the surface was only 0.1 wt%, the EPR signal characteristic of Ti^{3+} was not fully quenched, which implies that the defect sites were not saturated at this concentration. Consistent with this result, the IR spectra (Figure 6B) show that the OH band associated with the Ti^{3+} sites was not completely removed. Thus, we work from the hypothesis that all the rhenium on the surface at this low concentration was present at defect sites and infer that, with more precise and systematic experimentation, it would be possible to refine the methods to count the number of defect sites by titrating them with $[Re_3(CO)_{12}H_3]$. We caution that EPR, IR, and EXAFS data in combination would be required to distinguish the rhenium carbonyls at the defect sites from those present at other sites.

Thus, the EXAFS data characterizing the rhenium carbonyls at the lower loading are different from those characterizing the rhenium carbonyls at the higher loading. Specifically, the former are characterized by a shorter Re–O distance, indicating a stronger interaction of the clusters with the support than in the case of the higher rhenium loading. Furthermore, the Re–C and C–O distances characterizing the clusters present at the lower loading are close to those reported for $[Re_3(CO)_{12}H]^{2-}$ (Table 8), and the values are markedly different from those characterizing the rhenium carbonyls at the higher loading, which correspond to less deprotonated clusters (Table 8).[48,50]

In summary, the data show the rhenium clusters present at the lower loading of 0.1 wt% Re on the surface interact more strongly with the surface than those present at the higher loading, and further that the former are present at Ti^{3+} surface-defect sites, in which they are more highly deprotonated than the clusters on other sites. The stronger bonding of the rhenium carbonyls located at the Ti^{3+} defect sites is consistent with the greater electron density available for bonding to the carbonyl ligands in the deprotonated clusters.

Table 8. Comparison of Re–C and C–O bond lengths in $[Re_3(CO)_{12}H_x]^{x-3}$ ($x=1$–3) and in the supported rhenium carbonyls.

Sample/characterization method	Bond length [Å] Re-C	C-O	Ref.
$[Re_3(CO)_{12}H_3]$ /EXAFS spectroscopy	1.98	1.13	[50]
$[Re_3(CO)_{12}H_2]^-$ /EXAFS spectroscopy	1.92	1.18	[50]
$[Re_3(CO)_{12}H]^{2-}$ /XRD	1.83	1.24	[48]
1% Re on TiO_{2ox} formed from $[Re_3(CO)_{12}H_3]$ (model B)/EXAFS spectroscopy	1.93	1.17	this work
1% Re on TiO_{2vac} formed from $[Re_3(CO)_{12}H_3]$ (model B)/EXAFS spectroscopy	1.95	1.18	this work
0.1% Re on TiO_{2vac} formed from $[Re_3(CO)_{12}H_3]$ (model B)/EXAFS spectroscopy	1.81	1.32	this work

We propose a connection between the deprotonation of the rhenium carbonyls and the process of healing of the titania defect (Ti^{3+}) sites to which they are bound, as shown in Figure 10. Adsorption of $[Re_3(CO)_{12}H_3]$ on TiO_{2vac}, which had a relatively high density of surface-defect sites, led to the following: 1) a decrease in the number of Ti^{3+}–OH groups; 2) a decrease in the number of Ti^{3+} sites; 3) a decrease in the number of O^- radical species; and 4) an increase in the number of bridging OH groups.

These observations, made during the process of adsorption and deprotonation of $[Re_3(CO)_{12}H_3]$, are all explained by the representation shown in Figure 10 (but we do not rule out other possibilities).

We hypothesize that the changes take place at the oxygen vacancy sites located between Ti^{3+} sites incorporating OH groups and neighboring Ti^{4+} sites incorporating O^- radical species. When $[Re_3(CO)_{12}H_3]$ is adsorbed at the Ti^{3+} site and donates a proton to it, the proton interacts with the Ti^{4+}–O^- species, resulting in the formation of an OH group, which then becomes bonded to the Ti^{3+} site, thereby healing it and forming a bridging OH group as an O^- radical species is removed and the Ti^{3+} is converted to a Ti^{4+} site. Thus, the change involves the transformation of a Ti^{3+}–OH to a Ti^{4+}–OH group.

A limitation of this representation is that it accounts only for the reactions on single Ti^{3+} defect sites on titania, and it is known that other types of defect sites can exist, such as pairs of neighboring Ti^{3+} sites without O^- species. Our data do not distinguish such sites from the ones that we have attempted to model.

Conclusion

The IR, EPR, and EXAFS data reported here form the basis for a schematic representation of the surface chemistry of hydroxylated anatase. According to this picture, during evacuation at 723 K, defect sites are formed on hydroxylated titania as either 1) a bridging OH group is removed,

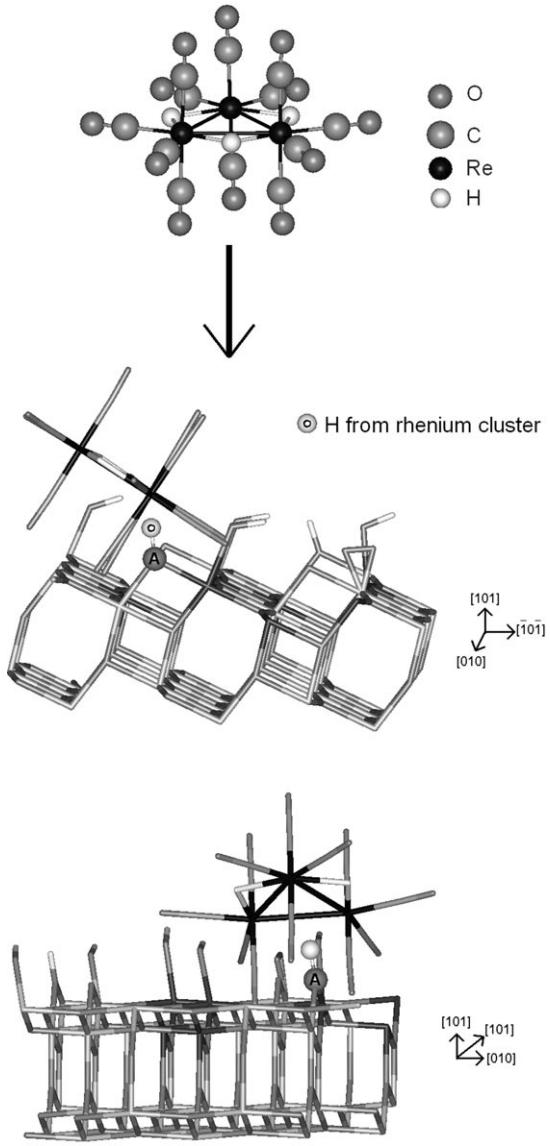

Figure 10. Representation of the anatase (101) surface upon adsorption of $[Re_3(CO)_{12}H_3]$.

forming two neighboring Ti^{3+} sites, or 2) when a Ti^{4+}–O bond is cleaved, forming a Ti^{3+} site and an O^- species, with the Ti^{4+}–OH group being converted into a Ti^{3+}–OH group. When the probe molecule $[Re_3(CO)_{12}H_3]$ is adsorbed on a titania surface incorporating Ti^{3+} defect sites, it reacts preferentially with these sites, becoming deprotonated, removing most of the oxygen radicals, and healing the defect sites.

Experimental Section

Materials: The following compounds were used in the synthesis of $[Re_3(CO)_{12}H_3]$: $Re_2(CO)_{10}$ (Pressure chemicals), $NaBH_4$ (+98%, Acros), tetrahydrofuran (THF, +99%, Sigma-Aldrich), phosphoric acid (85%, Sigma-Aldrich), and cyclohexane (99%, EM Science); *n*-pentane solvent (Fisher, 99%) was dried and purified by refluxing over sodium benzophenone ketyl and deoxygenated by sparging of N_2 (99.997%, Airgas). Titanium tetraisopropoxide ($Ti(OiPr)_4$, 99.999%) and anhydrous ethanol used in the synthesis of titania were supplied by Aldrich. The O_2 (99.7%) used for the treatment of the titania samples was supplied by Airgas.

Synthesis of titania: Anatase was synthesized by a sol–gel method with a water:alkoxide solvent mixture used in a molar ratio of 165:1.[64] $Ti(OiPr)_4$ was added to anhydrous ethanol, and the solution was added dropwise into a 50 vol% solution of ethanol in water. The resultant solution was then stirred at room temperature for 2 h; a precipitate formed, which was separated from the mother liquor by centrifugation and washed five times in ethanol (to minimize particle agglomeration) and dried overnight at room temperature. The resultant anatase powder was calcined for 4 h in flowing O_2 at 723 K.[65] The anatase crystal structure was confirmed by powder XRD.

TiO_2 samples were treated either in O_2 or under vacuum ($<10^{-3}$ mbar) at 723 K for 4 h. They were evacuated at room temperature and stored under N_2 in a glove box prior to characterization.

Synthesis of $[Re_3(CO)_{12}H_3]$: $[Re_3(CO)_{12}H_3]$ was synthesized from $Re_2(CO)_{10}$ by the method of Andrews et al.[66] All handling was done in a glove box or by using standard Schlenk techniques to minimize exposure to O_2 and moisture. $[Re_3(CO)_{12}H_3]$ was isolated by precipitation from a hot cyclohexane solution and washed with dry *n*-pentane and then stored in an N_2-filled glove box. The identity of the precursor in a CH_2Cl_2 was confirmed by IR spectra matching the literature spectrum.[38]

Preparation of titania incorporating rhenium carbonyls: The preparations and sample transfers were performed by using standard Schlenk techniques and an N_2-filled glove box. $[Re_3(CO)_{12}H_3]$ was adsorbed on each of the treated titania samples (TiO_{2ox} and TiO_{2vac}) by slurrying in *n*-pentane; each slurry was stirred at room temperature for 24 h and then evacuated at the same temperature for 24 h to remove the solvent. The resultant samples were stored under N_2 in a glove box until further use.

Methods

Powder X-ray diffraction: The anatase samples were transferred from the glove box and pressed into the sample holder in air. XRD patterns of the samples were collected with a Scintag XDS-2000 X-ray powder diffractometer by using filtered $Cu_{K\alpha}$ radiation ($\lambda = 1.541$ Å). Each reported pattern was obtained in the range of 10 to 80° with 0.02° scanning steps.

IR spectroscopy: Each powder sample was pressed between two KBr windows in the glove box and mounted into a sealed cell. IR spectra were collected for samples under vacuum with a Bruker IFS 66v spectrometer operated with a resolution of 2 cm^{-1}. Each reported spectrum is the average of 64 scans.

EPR spectroscopy: Samples were loaded into EPR tubes in the glove box and then evacuated overnight and flame sealed. Data were collected at the calEPR Center at the University of California, Davis, on a Bruker ECS 106 X-band spectrometer equipped with a Bruker ER4116DM cavity operating in the TE102 mode. Samples were cooled with liquid helium, and the temperature was controlled at 5 K with an Oxford ESR900 liquid helium cryostat equipped with an Oxford ITC503 temperature controller.

X-ray absorption spectroscopy: The powder samples formed by adsorption of $[Re_3(CO)_{12}H_3]$ on titania were characterized by X-ray absorption spectroscopy at the Re L_{III} edge (10535 eV). Data were collected in fluorescence mode at beamline X-18B of the National Synchrotron Light Source (NSLS) and at beam line 2–3 of the Stanford Synchrotron Radiation Laboratory (SSRL). Si(111) and Si(220) double-crystal monochromators were used at the respective synchrotrons, with respective spectral resolutions of 1 and 0.5 eV.

Samples in an argon-filled glove box were packed into a sample holder and sealed with Kapton tape. The measurements were done at room temperature with a N_2-filled ion chamber used to measure the incoming X-rays and a 13-element germanium detector used for the fluorescence; the germanium detector window was set for the L_α lines (8652 and 8586 eV). The monochromator was detuned 25% to suppress higher harmonics in the beam. The data in the EXAFS region were collected with an even grid of 0.07 *k* (*k* is the wave vector) and with a constant integration time. Some samples contained 1 wt% Re, and each of these was scanned at

least four times. One sample contained only 0.1 wt% Re, and it was scanned 10 times. The average collection time per scan was 30 min.

Analysis of IR spectra: Baseline removal was done with the software package OPUS by using a spline function. Data fitting was achieved by using a sum of Voigt-type functions. Convolution of the Voigt functions was done numerically by using Simpson's rule for integration. Newton's method was used for the least-squares optimizations. Initial guesses of peak positions were estimated directly form the spectra, and these were optimized in the fitting.

Analysis of EXAFS spectra: Data reduction and analysis were carried out with the average of all the scans taken for each sample, by use of the software XDAP.[47] The data were fitted to multiple-shell models with a difference file technique, with fitting done in both *R*- (distance) and *k*-space.[67] The objective function used for the least-squares fitting of the data is reported elsewhere.[67] Both the magnitude and the imaginary part of the Fourier transformed data were fitted with k^1, k^2, and k^3 weightings of the data until the fit was optimized. The software FEFF7[68] was used to determine amplitude- and phase-shift functions by theoretical calculations for reference materials with known crystal structures, except that experimental EXAFS results were used as a reference for Re–O contributions characterized by multiple scattering. The reference compounds used for each EXAFS contribution are summarized in Supporting Information.

The presence of low-Z scatterers at distances of approximately 3.0 Å from Re is an indication of carbonyl oxygen atoms (which are characterized by collinear multiple scattering with the carbonyl carbon atom). To distinguish such contributions from single-scattering contributions, phase- and amplitude-correction was used.[67] The identities of the other contributions were also confirmed by using phase and amplitude correction.

To estimate the value of the amplitude reduction factor in the EXAFS equation, S_0^2,[67] the EXAFS spectra characterizing the precursor $[Re_3(CO)_{12}H_3]$ were analyzed by fixing the values of interatomic distances and coordination numbers to those determined by crystallography[69] and allowing the values of S_0^2 to vary. The values of the inner potential correction, ΔE_0, and the Debye–Waller factor, $\Delta\sigma^2$, with respect to the reference material were also allowed to vary for each contribution in the determination of the value of S_0^2. A satisfactory value of S_0^2 of 0.91 was obtained.[70]

The number of fitted parameters for each model was justified statistically according to the criterion of the Nyquist theorem (Tables 5–7).[73] To estimate the statistical error associated with the $\chi(k)$ values for each data set (used in the estimation of precisions), the averaged data were Fourier filtered by using a *k*-window larger than that used for the data fitting and an *R*-range of 0–10 Å. The filtered data were then subtracted from the raw data to obtain an estimate of the error at each point. The root mean square error was calculated and used for calculation of precisions and the goodness of fit.

The precisions reported for each of the parameters in the EXAFS models were calculated on the basis of the objective function of the fitting routine.[67] The values of goodness of fit and of the $(\Delta\chi)^2$ function (recommended by the International XAFS Society[74]) were included with each fit.

Acknowledgements

This research was supported by the US Department of Energy, Office of Energy Research, Office of Basic Energy Sciences (Contract FG02–87ER13790) and the Thailand Research Fund. R.D.B. and the calEPR Center were supported by NIH (GM 48242, GM 73789, RR021075). We acknowledge the Stanford Synchrotron Radiation Laboratory, a national user facility operated by Stanford University on behalf of the US Department of Energy, Office of Basic Energy Sciences. The SSRL Structural Molecular Biology Program is supported by the Department of Energy, Office of Biological and Environmental Research, and by the National Institutes of Health, National Center for Research Resources, Biomedical Technology Program. We also acknowledge the National Synchrotron Light Source (NSLS), Brookhaven National Laboratory, for access to beam time; the NSLS is supported by the US Department of Energy, Office of Science, Office of Basic Energy Sciences, under Contract No. DE-AC02–98CH10886.

[1] A. Fujishima, K. Honda, *Nature* **1972**, *238*, 37–38.
[2] K. Suriye, P. Praserthdam, *Stud. Surf. Sci. Catal.* **2006**, *159*, 717- 720.
[3] Y. Ishikawa, Y. Matsumoto, Y. Nishida, S. Taniguchi, J. Watanabe, *J. Am. Chem. Soc.* **2003**, *125*, 6558–6562.
[4] K. Suriye, P. Praserthdam, B. Jongsomjit, *Ind. Eng. Chem. Res.* **2005**, *44*, 6599–6604.
[5] J. F. Goellner, B. C. Gates, *J. Phys. Chem. B* **2001**, *105*, 3261–3281.
[6] V. Henrich, R. L. Kurtz, *Phys. Rev. B* **1981**, *23*, 6280–6287.
[7] U. Diebold, *Surf. Sci. Rep.* **2003**, *48*, 53–229.
[8] G. Lu, A. Lingsebigler, J. T. Yates, Jr., *J. Phys. Chem.* **1994**, *98*, 11733–11738.
[9] S. Yamazaki, S. Tanaka, H. Tsukamoto, *J. Photochem. Photobiol. A* **1999**, *212*, 55–61.
[10] D. R. Park, J. Zhang, K. Ikeue, H. Yamashita, M. Anpo, *J. Catal.* **1999**, *185*, 114–119.
[11] K. Suriye, P. Praserthdam, B. Jongsomjit, *Appl. Surf. Sci.* **2007**, *253*, 3849–3855.
[12] C. N. Rusu, J. T. Yates Jr. , *Langmuir* **1997**, *13*, 4311–4316.
[13] T. L. Thomson, O. Diwald, J. T. Yates Jr. , *J. Phys. Chem. B* **2003**, *107*, 11700–11704.
[14] M. A. Henderson, W. S. Epling, C. H. F. Peden, C. L. Perkins, *J. Phys. Chem. B* **2003**, *107*, 534–545.
[15] Z. Zhang, S. P. Jeng, V. E. Henrich, *Phys. Rev. B* **1991**, *43*, 12004–12011.
[16] V. E. Henrich, G. Dresselhaus, H. J. Zeiger, *Phys. Rev. Lett.* **1976**, *36*, 1335–1339.
[17] L. Q. Wang, D. R. Baer, M. H. Engelhard, *Surf. Sci.* **1994**, *320*, 295–306.
[18] R. Wang, K. Hashimoto, A. Fujishima, M. Chikuni, E. Kojima, A. Kitamura, M. Shimohigoshi, T. Watanabe, *Adv. Mater.* **1998**, *10*, 135–138.
[19] Q. Zhong, J. M. Vohs, D. A. Bonnell, *Surfactant Sci. Ser.* **1992**, *274*, 35–43.
[20] W. Gopel, J. A. Anderson, D. Frankel, M. Jähnig, K. Phillips, J. A. Schafer, G. Rocker, *Surf. Sci.* **1984**, *139*, 333–346.
[21] J. M. Pan, B. L. Maschhoff, U. Diebold, T. E. Madey, *J. Vac. Sci. Technol. A* **1992**, *10*, 2470–2476.
[22] Y. Nakaoka, Y. Nosaka, *J. Photochem. Photobiol. A* **1997**, *110*, 299–305.
[23] S. Gan, Y. Liang, D. R. Baer, M. R. Sievers, G. S. Herman, C. H. F. Peden, *J. Phys. Chem. B* **2001**, *105*, 2412–2416.
[24] G. Li, L. Li, J. Boerio-Goates, B. F. Woodfield, *J. Am. Chem. Soc.* **2005**, *127*, 8659–8666.
[25] Y. Zhang, J. Li, J. Wang, *Chem. Mater.* **2006**, *18*, 2917–2923.
[26] J. M. Coronado, A. J. Maira, J. C. Conesa, K. L. Yeung, V. Augugliaro, J. Soria, *Langmuir* **2001**, *17*, 5368–5374.
[27] Y. Nakaoka, Y. Nosaka, *J. Photochem. Photobiol. A* **1997**, *110*, 299–305.
[28] W. Grunert, A. Brückner, H. Hofmeister, P. Claus, *J. Phys. Chem. B* **2004**, *108*, 5709.
[29] R. F. Howe, M. Grätzel, *J. Phys. Chem.* **1987**, *91*, 3906–3909.
[30] O. I. Micic, Y. Zhang, K. R. Cromack, A. D. Trifunac, M. C. Thurnauer, *J. Phys. Chem.* **1993**, *97*, 13284–13288.
[31] S. Zhang, W. Li, Z. Jin, J. Yang, J. Zhang, Z. Du, Z. Zhang, *J. Solid State Chem.* **2004**, *177*, 1365–1371.
[32] T. L. Thompson, J. T. Yates, Jr., *Chem. Rev.* **2006**, *106*, 4428–4453.
[33] X. Li, W. S. Jenks, *J. Am. Chem. Soc.* **2000**, *122*, 11864–11870.
[34] S. H. Szczepankiewicz, A. J. Colussi, M. R. Hoffman, *J. Phys. Chem. B* **2000**, *104*, 9842–9850.
[35] S. Mozia, M. Tomaszewska, B. Kosowska, B. Grzmil, A. W. Morawski, K. Kaucki, *Appl. Catal. B* **2005**, *55*, 195–200.
[36] A. S. Vuk, R. Jese, M. Gaberscek, B. Orel, G. Drazic, *Sol. Energy Mater. Sol. Cells* **2006**, *90*, 452–468.

[37] M. I. Zaki, M. A. Hasan, Al-Sagheer F. A.; L. Pasupulety, *Colloids Surf. A* **2001**, *190*, 261–274; L. Pasupulety, *Colloids Surf. A* **2001**, *190*, 261–274.
[38] U. A. Jayasooriya, S. J. Stotesbury, R. Grinter, D. B. Powell, N. Sheppard, *Inorg. Chem.* **1986**, *25*, 2853–2857.
[39] P. S. Kirlin, F. A. DeThomas, J. W. Bailey, H. S. Gold, C. Dybowski, B. C. Gates, *J. Phys. Chem.* **1986**, *90*, 4882–4887.
[40] J. F. Goellner, B. C. Gates, Vayssilov, N. G. N. Rösch, *J. Am. Chem. Soc.* **2000**, *122*, 8056–8066.
[41] A comparison of Figure 4B and C suggests that the result of the adsorption was the same for both TiO_{2vac} and TiO_{2ox} when the loading was 1.0 wt% Re. The spectrum of the sample containing 0.1 wt% Re exhibits a shift with respect to the spectrum of the samples containing 1.0 wt% Re, suggesting that the species formed upon adsorption in the sample with 0.1 wt% Re is different from those produced with 1.0 wt% Re. These results are broadly consistent with what was observed by EXAFS. The EXAFS results suggest that the shift of the peak at approximately 1977 cm^{-1} was related to the degree of deprotonation of the cluster; however, the small shifts could also be a consequence of small changes in the environment as the cluster is placed either in solution or on the surface.
[42] Adsorption of $[Re_3(CO)_{12}H_3]$ on TiO_{2vac} led to a band at 3610 cm^{-1}. The position of this band matches to that of gas-phase H_2O_2.[43] Connor et al.[44] assigned the nearby band at 3600 cm^{-1} to OH groups weakly bonded to titania; thus, the assignment of this band is still debated. These observations are consistent with those of Szczepankiewiez et al.,[34] who observed a band at 3610 cm^{-1} characterizing a titania sample that had been treated under vacuum at high temperature and then exposed to HCl; however, they did not assign the band. The observed decrease in the number of O_2^- species and the appearance of the band at 3610 cm^{-1} might be explained as a result of another reaction with $[Re_3(CO)_{12}H_3]$, as follows: The proton could interact with O_2^- to form HO_2, which could be converted into other products.[45] Nakamura et al.[46] reported that O_2^- in acidic solutions reacted to give such an intermediate and then to H_2O_2.
[43] R. L. Miller, D. F. Hornig, *J. Chem. Phys.* **1961**, *34*, 265–272.
[44] P. A. Connor, K. D. Dobson, A. J. McQuillan, *Langmuir* **1999**, *15*, 2402–2408.
[45] T. Scheiring, A. Klein, W. Kaim, *J. Chem. Soc. Perkin Trans. 1* **1997**, *2*, 2569–2571.
[46] R. Nakamura, A. Imanishi, K. Murakoshi, Y. Nakato, *J. Am. Chem. Soc.* **2003**, *125*, 7443–7450.
[47] M. Vaarkamp, J. C. Linders, D. C. Koningsberger, *Physica B* **1995**, *208-209*, 159–160.
[48] G. Ciani, G. D'Alfonso, M. Freni, P. Romiti, A. Sironi, *J. Organomet. Chem.* **1978**, *157*, 199–208.
[49] M. A. Henderson, *Langmuir* **1996**, *12*, 5093–5098.
[50] F. B. M. van Zon, P. S. Kirlin, B. C. Gates, D. C. Koningsberger, *J. Phys. Chem.* **1989**, *93*, 2218–2222.
[51] A. S. Fung, P. A. Tooley, M. J. Kelley, D. C. Koningsberger, B. C. Gates, *J. Phys. Chem.* **1991**, *95*, 225–234.
[52] F. Guillemot, M. C. Porte, C. Labrugere, Ch. Baquey, *J. Colloid Interface Sci.* **2002**, *255*, 75–78.
[53] Q. Guo, I. Cocks, E. M. Williams, *Phys. Rev. Lett.* **1996**, *77*, 3851–3854.
[54] A. Szabo, T. Engel, *Surf. Sci.* **1995**, *329*, 241–254.
[55] P. J. Moller, M. C. Wu, *Surf. Sci.* **1989**, *224*, 265–276.
[56] A. Vittadini, A. Selloni, F. P. Rotzinger, M. Grätzel, *Phys. Rev. Lett.* **1998**, *81*, 2954–2957.
[57] A. Tilocca, A. Selloni, *Langmuir* **2004**, *20*, 8379–8384.
[58] A. Tilocca, A. Selloni, *J. Phys. Chem. B* **2004**, *108*, 4743–4751.
[59] G. S. Herman, Z. Dohnalek, N. Ruzycki, U. Diebold, *J. Phys. Chem. B* **2003**, *107*, 2788–2795.
[60] A. Tilocca, A. Selloni, *J. Chem. Phys.* **2003**, *119*, 7445–7450.
[61] E. Carter, A. F. Carley, D. M. Murphy, *J. Phys. Chem. C* **2007**, *111*, 10630–10638.
[62] The plausibility of this inference is supported by calculations at the level of density functional theory[63] showing that a minimum-energy configuration corresponds to an O_2^- species located at a five-fold coordinated Ti^{4+} site (Figure 9).
[63] G. Mattioli, F. Filippone, A. A. Bonapasta, *J. Am. Chem. Soc.* **2006**, *128*, 13772–13780.
[64] C. C. Wang, J. Y. Ying, *Chem. Mater.* **1999**, *11*, 3113–3120.
[65] The as-synthesised TiO_2 powder still contained residues from the synthesis (mainly 2-propanol, $Ti(OPr)_4$, ethanol, and water); however, after the initial calcination at 723 K, any of these residues are expected to have been removed or reacted away (which has been associated with the formation of defects observed in the TiO_2 sample[11]). No evidence of impurities was observed in the IR spectra of the sample after initial calcination. Furthermore, the formation of O^- and O_2^- species suggests that the defects were formed from the desorption of water and not from the desorption of impurities.
[66] M. A. Andrews, S. W. Kirtley, H. D. Kaesz, *Inorg. Synth.* **1977**, *17*, 66–68.
[67] D. C. Koningsberger, B. L. Mojet, G. E. van Dorssen, D. E. Ramaker, *Top. Catal.* **2000**, *10*, 143–155.
[68] A. L. Ankudinov, J. J. Rehr, *Phys. Rev. B* **1997**, *56*, R1712.
[69] N. Masciocchi, A. Sironi, G. D'Alfonso, *J. Am. Chem. Soc.* **1990**, *112*, 9395–9397.
[70] In the past appropriate values of S_0^2 were thought to be in the range of 0.7–0.8;[71] however, more recently, values in the range of 0.7–1.0 are considered to be appropriate.[72]
[71] D. C. Koningsberger, R. Prins, X-ray Absorption: Principles, Applications, Techniques of EXAFS, SEXAFS, and XANES; Wiley: New York, **1988**.
[72] Tutorial on: Fundamentals of X-ray Absorption Fine Structure. http://xafs.org/Tutorials?action=AttachFile&do=get&target=Newville_Intro.pdf (accessed Feb 2006).
[73] E. A. Stern, *Phys. Rev. B* **1993**, *48*, 9825–9827.
[74] International XAFS Society, Error Reporting Recommendations: A Report of the Standards and Criteria Committee. http://fisica.unicam.it/IXS/OLD/subcommittee_reports/sc/err-rep.pdf (accessed Feb 2006).

Received: September 25, 2007
Published online: January 10, 2008

